Applied Physics Letters

Increase of Néel temperature of magnetoelectric Cr_2O_3 thin film by epitaxial lattice matching

Cite as: Appl. Phys. Lett. **121**, 182402 (2022); https://doi.org/10.1063/5.0116968
Submitted: 30 July 2022 • Accepted: 10 October 2022 • Published Online: 01 November 2022

Xinrui Wang, Kakeru Ujimoto, Kentaro Toyoki, et al.

Applied Physics Letters ARTICLE scitation.org/journal/apl

Increase of Néel temperature of magnetoelectric Cr_2O_3 thin film by epitaxial lattice matching

Cite as: Appl. Phys. Lett. **121**, 182402 (2022); doi: 10.1063/5.0116968
Submitted: 30 July 2022 · Accepted: 10 October 2022 ·
Published Online: 1 November 2022

Xinrui Wang,[1] Kakeru Ujimoto,[1] Kentaro Toyoki,[1,2,3] Ryoichi Nakatani,[1,2,3] and Yu Shiratsuchi[1,2,3,a)]

AFFILIATIONS

[1]Department of Materials Science and Engineering, Graduate School of Engineering, Osaka University, 2-1 Yamadaoka, Suita, Osaka 5650871, Japan
[2]Division of Spintronics Research Network, Institute for Open and Transdisciplinary Research Initiatives, Osaka University, 2-1 Yamadaoka, Suita, Osaka 565-0871, Japan
[3]Center for Spintronics Research Network, Graduate School of Engineering Science, Osaka University, 1-3 Machikaneyama, Toyonaka 560-8531, Japan

[a)]Author to whom correspondence should be addressed: shiratsuchi@mat.eng.osaka-u.ac.jp

ABSTRACT

Increase in the Néel temperature (T_N) of the 10-nm thick Cr_2O_3(0001) thin films by the lattice strain was experimentally investigated. T_N was determined based on the zero-offset anomalous Hall measurements for the Pt/Cr_2O_3/Pt epitaxial trilayer. The lattice strain was altered by the Pt buffer layer thickness and was evaluated by the lattice parameters. T_N was increased from 241.5 to 260.0 K by varying the Pt buffer layer thickness from 0 to 20 nm. For the film without the Pt buffer layer, the apparent critical exponent near T_N increased suggesting the distribution of T_N due to the inhomogeneous strain. The T_N value was weakly correlated with the axial ratio c/a and the lattice volume of the Cr_2O_3 layer V; T_N increases with decreasing c/a or increasing V. The increase in T_N by the reduction in c/a (or by increasing V) implies that the exchange coupling between the nearest neighbor Cr^{3+} spins has the significant role in the strain effect.

Antiferromagnetic (AFM) spintronics has been an area of active pursuit, where a variety of unique features of antiferromagnet such as the robustness against the external magnetic field and the ultrafast spin precession are enjoyed.[1] The Néel temperature T_N is a characteristic temperature of antiferromagnet; below T_N, the AFM ordering appears. In the viewpoint of the AFM spintronics devices, T_N limits the operation temperature, and the increase in T_N is desired. T_N is determined by the exchange coupling constants between the AFM spins, and the strength of the exchange coupling constants depends on the bond distance and/or the bond angle between the AFM spins. Consequently, T_N can change depending on the lattice deformation by an external/internal stress (or strain) and/or the lattice parameters.[2,3]

There are examples of the attempts to alter T_N of the magnetoelectric (ME) Cr_2O_3,[4–14] a promising candidate to realize the voltage-driven AFM spintronic device.[14,15] In Fig. 1, the Cr^{3+} alignment in the $\langle 11\bar{2}0\rangle$-projection and the spin alignment within the Cr_2O_3 unit cell are shown. Cr^{3+} spins alternatively align along the c-axis in the hexagonal cell, which is $\langle 111\rangle$ in the rhombohedral cell. J_1 and J_2, the exchange coupling between first and second nearest neighbor Cr^{3+} spins, respectively, has a significant role on the effective exchange J. Although J_2 is about half of J_1 in magnitude, J_2 has a nonnegligible role on J because the number of bonds for J_2 is more than that for J_1; 1 for J_1 and 3 for J_2, respectively.[17] Historically, there are controversial reports for the stress-effect on T_N of Cr_2O_3. Some reports showed the increase in T_N under the hydrostatic pressure and the resultant compressive lattice deformation[5,6,12,13] and there are also the reports showing the opposite result, i.e., the reduction in T_N by the hydrostatic pressure.[4,7] Theoretical calculation also showed the controversial results.[9,10,13,14] Kota *et al.* predicted the increase in T_N or J by the tensile strain along the c axis, i.e., the increase in the axial ratio c/a,[9,10,13] whereas Mu and Belashchenko predicted the opposite trends, the decrease in J, proportional to T_N with decreasing c/a.[14] Although the previous experimental attempts were done for the bulk Cr_2O_3, the attempt for the Cr_2O_3 thin film is more impressive for the device application since one concern of the ME-control of AFM spin state of the Cr_2O_3 thin film is the low operation temperature.[11,16] In the epitaxial thin film, the strain can apply to the film via the lattice matching with the adjacent layer. Previously, we fabricated the epitaxial Pt/Cr_2O_3/Pt epitaxial trilayer and demonstrated that T_N could be detected by the anomalous Hall effect (AHE).[18] In this paper, we alter the Pt

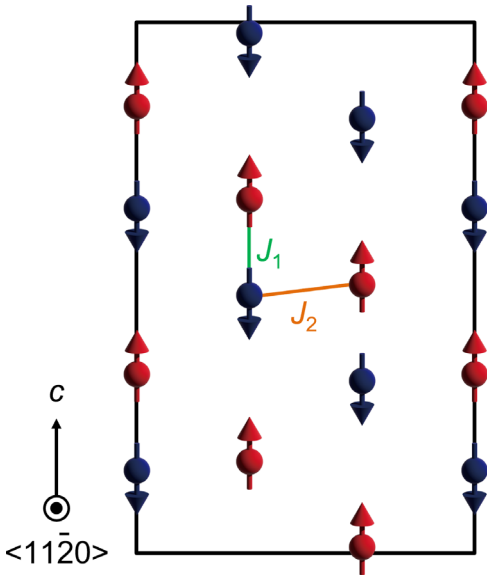

FIG. 1. $\langle 11\bar{2}0\rangle$-projected Cr^{3+} arrangement with the spin orientation in the Cr_2O_3. Exchange coupling constants for first and second nearest-neighbor Cr^{3+} spins, i.e., J_1 and J_2 are also shown.

buffer layer thickness to change the epitaxial strain applied to the Cr_2O_3 layer and investigated the influence on T_N. We demonstrate the increase in T_N, $\Delta T_N \sim 20$ K for the 10-nm-thick Cr_2O_3 layer by changing the Pt buffer layer thickness.

Pt(2 nm)/Cr_2O_3(10 nm)/Pt(t_{Pt} nm) triyalers were used as the sample. t_{Pt} was varies as 0, 3, 8, 16, 18, and 20. The cleaned α-Al_2O_3(0001) single crystal was used as the substrate. The films were fabricated by the DC magnetron sputtering system with the base pressure below 1×10^{-6} Pa. The detailed sample fabrication method can be found in our previous report.[18] Structural characteristics were evaluated by using reflection high-energy electron diffraction (RHEED) and high-angle x-ray diffraction (XRD). Typical RHEED patterns for each layer are shown in Fig. 2. The equally spaced streaks are observed indicating that the crystallographic orientation along the growth direction is aligned. The appearance of streaks indicates the flat surface of each layer. Some RHEED images, e.g., Pt for $[1\bar{1}00]_{subst}$-azimuth and Cr_2O_3 for $[11\bar{2}0]_{subst}$-azimuth, are symmetric with respect to (00) streak indicting the twin formation. Resultantly, the epitaxial relationship of each layer is represented as

$$\begin{aligned}&Pt(111)[11\bar{2}] \,||\, Cr_2O_3(0001)[11\bar{2}0]\\ &\quad (||Pt(111)[11\bar{2}])||\alpha\text{–}Al_2O_3(0001)\,[11\bar{2}0]\\ &Pt(111)[1\bar{1}0] \,||\, Cr_2O_3(0001)[1\bar{1}00]\\ &\quad (||Pt(111)[1\bar{1}0])||\alpha\text{–}Al_2O_3(0001)\,[1\bar{1}00].\end{aligned}$$

The XRD measurements were done for the various configuration to capture the off-axis x-ray diffractions from the Cr_2O_3 layer to determine the lattice parameters, a and c of the Cr_2O_3 layer. Magnetic properties were characterized based on the AHE measurements. For the AHE measurements, the films were patterned into the Hall device with 25 μm length and 5 μm wide by using the photolithography and the Ar ion milling. After the patterning, the Au/Cr electrodes were prepared by the lift-off technique. The AHE measurements were done by the zero-offset method[19] using the multiplexer. The optical microscope image of the device and the schematic electric circuit are shown in Fig. 3. For the temperature dependent measurements, the sample was cooled from 310 to 10 K with the applied field of +2. After

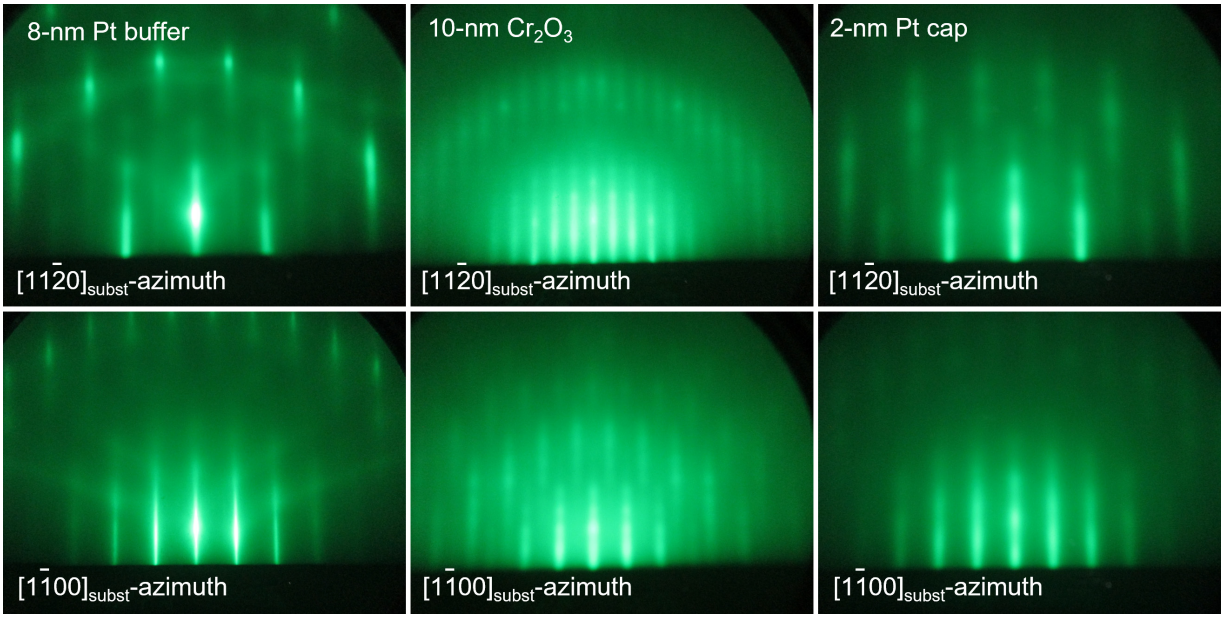

FIG. 2. RHHED images of (a) Pt buffer layer, (b) Cr_2O_3 layer, and (c) Pt capping layer. Electron azimuth was $\langle 11\bar{2}0\rangle$ (top panel) and $\langle 1\bar{1}00\rangle$ (bottom panel) of the α-Al_2O_3(0001) substrate, respectively. In this figure, the results for the case of $t_{PT} = 8$ nm are shown as examples.

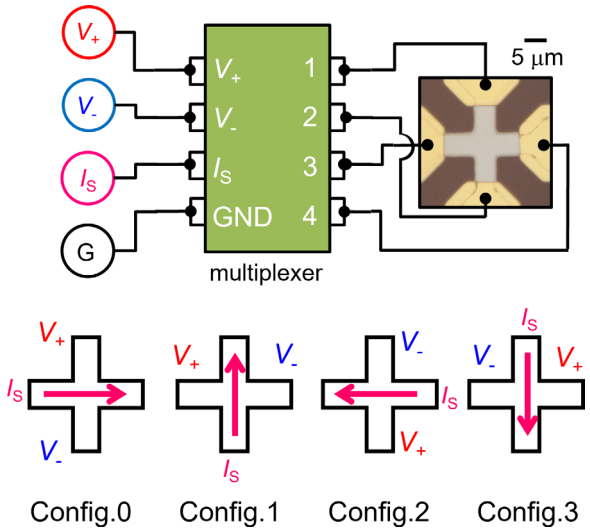

FIG. 3. Optical microscope image of the Hall device with the electric circuit used for the zero-offset Hall measurements.

stabilizing temperature, the magnetic field was removed. Upon increasing temperature, the AHE voltage was measured as a function of temperature; the remanent AHE voltage, V_{AHE_R}, was measured. The applied magnetic field direction was perpendicular to the film plane. The sense current I_s for the AHE measurements was 0.5 mA. Resistivity of the Cr_2O_3 layer was about 1 MΩ·m at room temperature, sufficiently high to expect the spintronic applications.

AHE for the Pt/Cr_2O_3 system is a recent research subject, and some possible origins are proposed.[19–22] Characteristics of AHE for this system is the nonlinear response as a function of the magnetic field above T_N[19–21] and the finite remanent AHE signal below T_N.[19] We confirmed that both characteristics appeared in every film. The nonlinear magnetic response above T_N is presented in the supplementary material. Figure 4(a) shows the temperature dependence of the remanent AHE resistance, $R_{AHE\_R} = V_{AHE\_R}/I_s$. The negative value of R_{AHE_R} at the positive cooling field is obtained. According to our adopted electric circuit shown in Fig. 3, the sign of R_{AHE_R} agrees with the previous reports.[18,19] As a trend, $|R_{AHE\_R}|$ increases with increasing temperature, shows the maximum, and decreases again. Finally, R_{AHE_R} becomes zero. The similar temperature dependence of R_{AHE_R} was reported in the previous reports for the Pt/40-nm thick Cr_2O_3/Pt trilayer.[19] The first increase in $|R_{AHE\_R}|$ in the low temperature regime is most prominent for the film with $t_{Pt} = 8$ nm, wherein the sign reversal of R_{AHE_R} takes place. This should not be simply attributed to the temperature dependence of sublattice magnetization,[23,24] but the similar feature has been observed in other system such as $SrRuO_3$,[25,26] $La_{1-x}Sr_xCoO_3$,[27] and Mn_3NiN,[28] where the AHE is caused by the complex mechanism involved by the Berry curvature or the spin-chiral texture. Moreover, the film with $t_{Pt} = 8$ nm shows the steep dip of R_{AHE_R} near T_N. Although the mechanism of this dip is not clear at present, the similar phenomenon has been observed in $SrRuO_3$ and $Sr_{0.8}Ca_{0.2}RuO_3$.[25,26] Our results imply that the AHE in the Pt/Cr_2O_3 system below T_N is relevant to the emergence of the Berry curvature as predicted in our previous report.[22] The ME effect might be also

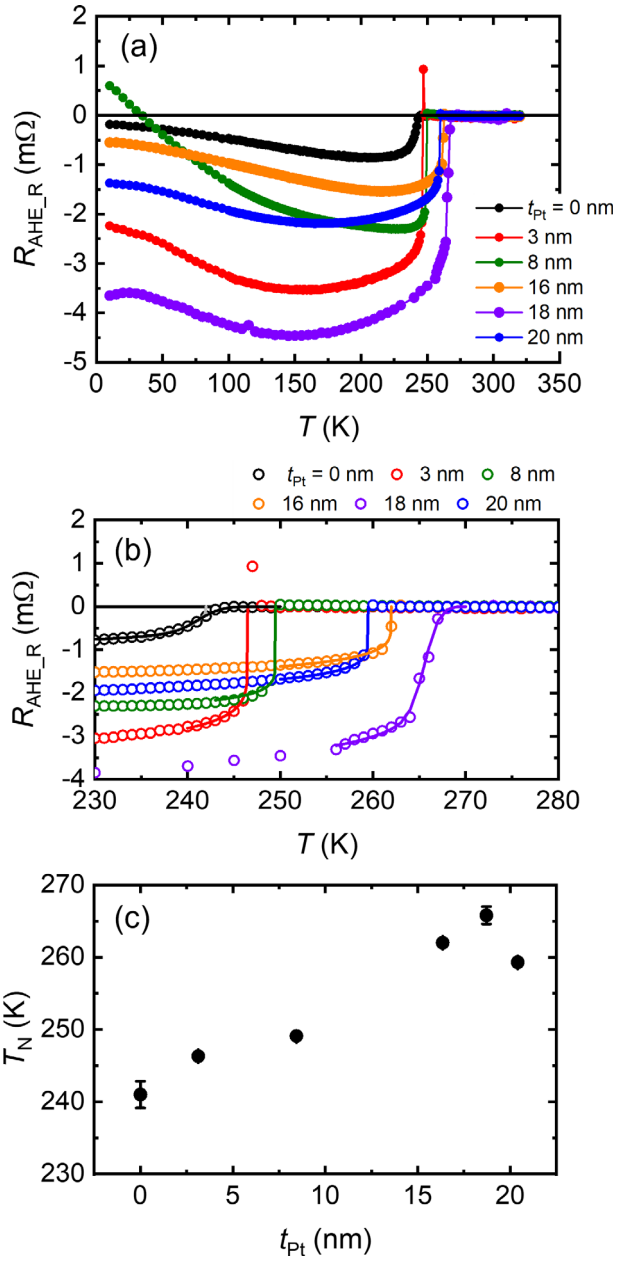

FIG. 4. (a) Temperature dependence of R_{AHE_E} for the films with $t_{Pt} = 0$ (black), 3 (red), 8 (green), 16 (orange), 18 (purple), and 20 (blue) nm. (b) Enlarged image of (a) in the temperature range of 230–270 K. Open circles represent the experimental results and the solid lines represent the fitted results. Gray and black lines for the film with $t_{Pt} = 0$ nm represent the fitted results using Eqs. (1) and (2), respectively. For other films, the fitting was done using Eq. (1). (c) Change in T_N with t_{Pt}.

relevant to the negative temperature coefficient of R_{AHE} as in the case of the Faraday rotation of the bulk Cr_2O_3.[29] Unfortunately, the relationship between the AHE and the ME effect has not been so far explored. Future exploration from both theory and experiments are expected. In this paper, we do not go into the further details of the

origin of AHE, and we focused on the change in T_N with t_{Pt} with the hypothesis that the remanent AHE is relevant to the AFM order parameter regardless of the detailed origin of AHE.

T_N was determined from the R_{AHE_R}–T curve by the power-law expressed by

$$R_{AHE_R}(T) = R_{AHE_R}(0)\left(1 - \frac{T}{T_N}\right)^{\beta}, \quad (1)$$

where $R_{AHE}(0)$ is the pre-factor and β is the critical exponent. In principle, the AHE conductivity $\sigma_{xy} = -\rho_{xy}/\rho_{xx}^2$ should be used for the fitting rather than R_{AHE_R}. Nonetheless, by restricting the temperature regime for the fitting to sufficiently small where ρ_{xx} is treated as constant, T_N can be estimated. We confirmed that T_N and β values are same if we used σ_{xy}. According to Figs. 4(a) and 4(b), R_{AHE_R} gradually changes for $t_{Pt} = 0$ nm compared with other films. When we fit the results simply using Eq. (1), β is estimated as 0.37 for $t_{Pt} = 0$ nm and ~0.13 for other t_{Pt}. $\beta \sim 0.13$ is similar to the two-dimensional (2D) Ising model, $\beta = 0.125$.[30] This implies that the 2D behavior of the interfacial Cr^{3+} spins, e.g., the boundary magnetization (the surface magnetization)[31,32] dominates the critical behavior. The gradual decrease in R_{AHE_R} and the increase in the apparent β for $t_{Pt} = 0$ can be alternated by assuming the distribution of T_N. As seen in Fig. 4(b), the fitted results using Eq. (1) cannot reproduce R_{AHE_R} very near T_N (gray line). Taking into account the T_N distribution,[33] Eq. (1) is replaced by the rounded power law

$$R_{AHE_R}(T) = \frac{R_{AHE_R}(0)}{\sqrt{2\pi}\delta_{T_N}} \int_0^{\infty} t_0^{\beta} \exp\left[-\frac{(T - T_N)^2}{2\delta_{T_N}^2}\right] dT_N$$
$$t_0 = \begin{cases} 1 - \dfrac{T}{T_N} & for\ T < T_N \\ 0 & for\ T \geq T_N \end{cases}. \quad (2)$$

The normal distribution is assumed as the distribution function of T_N. As seen in Fig. 4(b), Eq. (2) well reproduces the skirt of R_{AHE_R} (black line). The fitting revealed that the mean T_N and the standard deviation was 241.5 and 1.5 K, respectively, for the film with $t_{Pt} = 0$ nm by assuming $\beta = 0.125$. Figure 4(c) shows the change in T_N with t_{Pt}. T_N increases from 241.5 to 260 K with increasing t_{Pt} from 0 to 20 nm. The T_N values are lower than the bulk value (~310 K)[23] and the 20, 130, 250, and 500-nm thick Cr_2O_3 film (~290–300 K).[19,34–36] In order to briefly address the reduction in T_N, we checked T_N for the thick Cr_2O_3 (40 and 200 nm) films. The estimated T_N were 284.7 ± 0.6 and 288.9 ± 0.6 K for 40 and 200 nm thick films, respectively (see the supplementary material). T_N is going to recover the bulk value although they are still lower than the bulk indicating that T_N gently decreases with the decreasing Cr_2O_3 thickness, and thus, the low T_N in the 10-nm thick Cr_2O_3 should be due to the thickness effect. We also briefly note that the best fits for the thick films were obtained by assuming $\beta = 0.325$ as in the case of Refs. 17 and 18. The decrease in β in the mainly used films implies that the 2D fashion is pronounced by decreasing Cr_2O_3 thickness. To obtain the deep insight on the thickness dependence of T_N and the possible dimensional crossover, the detailed Cr_2O_3 thickness dependence is required. This is beyond the scope of this paper and will be discussed elsewhere.

In the following, we discuss the change in T_N with t_{Pt} in the viewpoint of the lattice strain in the Cr_2O_3 layer. The lattice strain is discussed based on the lattice parameters of the Cr_2O_3(0001) layer. Figures 5(a) and 5(b) show the in-plane XRD profiles, ($2\theta_\chi/\varphi$ profiles) along [11$\bar{2}$0] and [10$\bar{1}$0] of α-Al_2O_3(0001) substrate, respectively, for some films. In the $2\theta_\chi/\varphi$ profiles along [11$\bar{2}$0], the diffraction peaks from the Cr_2O_3 layer and the substrate are observed. The diffraction peaks from the Pt layer are absent because the diffraction angle of the possible {224} diffractions is in the high $2\theta_\chi/\varphi$ regime, ~147°. In the $2\theta_\chi/\varphi$ profiles along [10$\bar{1}$0], the diffraction peak originated from Cr_2O_3(30$\bar{3}$0) is observed. In this profile, the diffraction peak from Pt(220) for the non-zero t_{Pt} and that from α-Al_2O_3(30$\bar{3}$0) for $t_{Pt} = 0$ nm were also observed. The diffraction peak position for the Cr_2O_3 layer varies with t_{Pt} indicating that the lattice constants vary

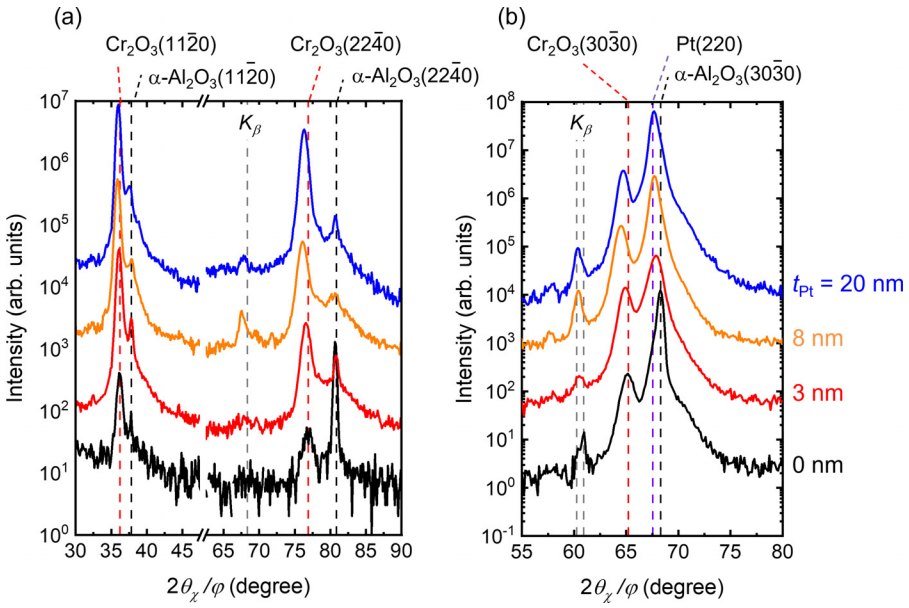

FIG. 5. $2\theta_\chi/\varphi$ profiles for the scattering vector along (a) [11$\bar{2}$0] and (b) [10$\bar{1}$0] of the α-Al_2O_3(0001) substrate.

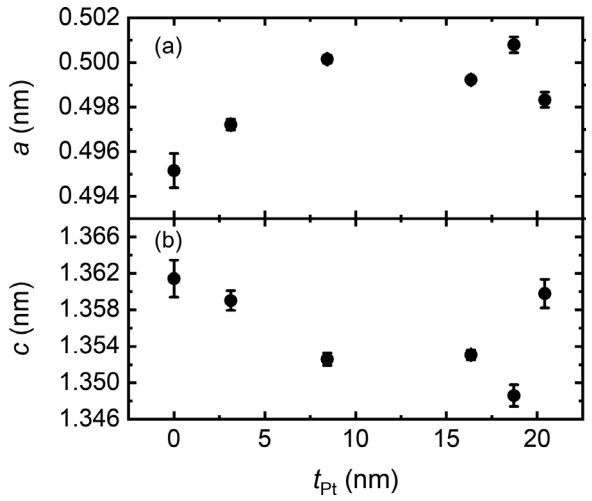

FIG. 6. Changes in lattice parameters (a) *a* and (b) *c* with t_{Pt}.

with t_{Pt}. For the precise determination of the lattice parameters, the off-axis XRD measurements, such as $(\bar{2}4\bar{2}6)$, $(\bar{1}2\bar{1}6)$, and $(2\bar{1}\bar{1}9)$ diffractions, were carried out. Using various diffraction peaks, the lattice parameters were estimated based on the Cohen's method[37] with the error function proportional to $\cos^2\theta \sin\theta$. It should be noted that the out-of-plane lattice spacing of $Cr_2O_3(0001)$ is difficult to directly evaluate, especially for the film with the Pt buffer layer, from the conventional out-of-plane $2\theta/\omega$ scan because the lattice spacing of Pt(111) is very near.

The changes in the lattice parameters of the Cr_2O_3 layer with t_{Pt} are shown in Fig. 6. *a* (*c*) increases (decreases) with the increasing t_{Pt} up to 8 nm. *a* (*c*) seems to gradually decrease (increase) above 8 nm and approaches *a* (*c*) or the thick (200 nm) Cr_2O_3 on the Pt buffer layer,[38] which suggests the partial relaxation of the lattice strain. Although the lattice parameters for $t_{Pt} = 0$ nm are almost same as the bulk lattice constants,[38,39] the errors mainly originating from the dispersion of the diffraction peak positions are large compared with other films. This suggests the inhomogeneity of the lattice strain in agreement with the rounded temperature dependence of R_{AHE_R} and that the steepening of R_{AHE_R}–T curve by the Pt buffer layer is relevant to the homogenization of the lattice strain. Combining Figs. 4(c) and 6, the relationships of T_N with *c*/*a* and lattice volume V $(=\sqrt{3}a^2c/2)$ are shown in Figs. 7(a) and 7(b), respectively. T_N increases with decreasing *c*/*a* or increasing V. These trends are in agreement with the recent theoretical prediction by Mu and Belaschanko.[14] They predicted that the lattice expansion along *a*-axis and the compression along *c*-axis, i.e., the decrease in *c*/*a* would cause the increase in J between the Cr^{3+} spins, which yields the increase in T_N. A 10% enhancement of J by a 1% in-plane tensile stress was predicted, which seems to be comparable to the results shown in Fig. 7(b), ~10% increase in T_N by ~2% decrease in *c*/*a*.

In summary, we investigated T_N of the $Cr_2O_3(0001)$ thin film in the $Pt/Cr_2O_3/Pt$ epitaxial trilayers based on the temperature dependence of R_{AHE_R}. When the Cr_2O_3 layer is deposited on the Pt buffer layer, R_{AHE_R} steeply decreases in the vicinity of T_N, which gives rise to the reduction in the critical exponent β. The estimated β (~0.125)

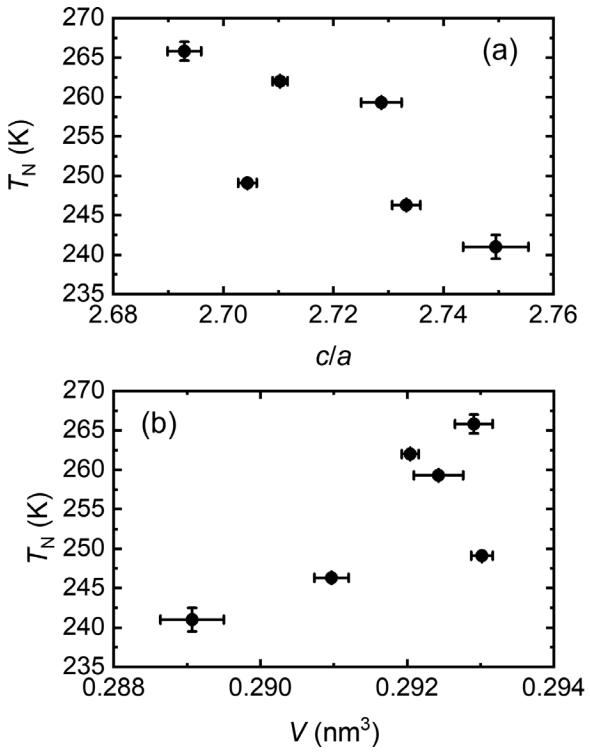

FIG. 7. Changes in T_N with (a) *c*/*a* and (b) lattice volume *V*.

implies the 2D Ising behavior of the interfacial AFM moments. T_N changes with the Pt buffer layer thickness and increases from 241.5 to 260.0 K with increasing t_{Pt}. T_N seems to be correlated with the axial ratio *c*/*a* and the lattice volume of the Cr_2O_3 layer. The enhancement ratio is comparable to the theoretical prediction.[14] The results suggest that the operation temperature of the magnetoelectric effect of the Cr_2O_3 layer can increase by the interface engineering, i.e., the suitable design of the stacking structure.

See the supplementary material for AHE loops measured at 300 K, i.e., above T_N for the studied films are presented (Sec. 1) and the supporting discussion of β for the thick Cr_2O_3 films (Sec. 2).

This work was partly supported by JSPS KAKENHI (Project Nos. 22H01757 and 22K18903), Iketani Science and Technology Foundation. The microfabrication was performed at the Photonics Center, Osaka University.

AUTHOR DECLARATIONS

Conflict of Interest

The authors have no conflicts to disclose.

Author Contributions

Xinrui Wang: Data curation (equal); Formal analysis (equal); Investigation (equal). **Kakeru Ujimoto:** Data curation (equal); Formal

analysis (equal); Investigation (equal); Writing – review & editing (equal). **Kentaro Toyoki:** Data curation (equal); Formal analysis (equal); Investigation (equal); Methodology (equal); Writing – original draft (equal); Writing – review & editing (equal). **Ryoichi Nakatani:** Investigation (equal); Supervision (equal); Writing – review & editing (equal). **Yu Shiratsuchi:** Conceptualization (lead); Formal analysis (equal); Funding acquisition (lead); Investigation (equal); Methodology (lead); Supervision (equal); Writing – original draft (lead); Writing – review & editing (lead).

DATA AVAILABILITY

The data that support the finding of this study are available from the corresponding author upon reasonable request.

REFERENCES

[1]T. Jungwirth, X. Marti, P. Wadley, and J. Wunderlich, Nat. Nanotechnol. **11**, 231 (2016).
[2]R. D. Goodenough, C. Isci, and S. B. Palmer, Physica B **86–88**, 61 (1977).
[3]I. S. Williams and R. Street, Philos. Mag. B **43**, 955 (1981).
[4]T. Wolton, R. Brugger, and R. Bennion, J. Phys. Chem. Solids **29**, 435 (1968).
[5]G. Gorodetsky, R. M. Hornreich, and S. Shtrikmam, Phys. Rev. Lett. **31**, 938 (1973).
[6]H. L. Alberts, J. Phys. Soc. Jpn. **38**, 1541 (1975).
[7]L. Bayajargal and B. Winkler, Appl. Phys. Lett. **102**, 182403 (2013).
[8]S. Mu, A. L. Wyscoki, and K. D. Belashchenko, Phys. Rev. B **87**, 054435 (2013).
[9]Y. Kota, H. Imamura, and M. Sasaki, Appl. Phys. Express **6**, 113007 (2013).
[10]Y. Kota, H. Imamura, and M. Sasaki, J. Appl. Phys. **115**, 17D719 (2014).
[11]M. Street, W. Echtenkamp, T. Komesu, S. Cao, P. A. Dowben, and C. Binek, Appl. Phys. Lett. **104**, 222402 (2014).
[12]N. O. Golosova, D. P. Kozlenko, S. E. Lukin, H.-P. Liermann, K. V. Glazyrin, and B. N. Savenko, J. Alloys Compd. **722**, 593 (2017).
[13]Y. Kota, Y. Yoshimori, H. Imamura, and T. Kimura, Appl. Phys. Lett. **110**, 042902 (2017).
[14]S. Mu and K. D. Belashchenko, Phys. Rev. Mater. **3**, 034405 (2019).
[15]X. He, Y. Wang, N. Wu, A. N. Caruso, E. Voscovo, K. D. Belashchenko, P. A. Dowben, and C. Binek, Nat. Mater. **9**, 579 (2010).
[16]Y. Shiratsuchi, K. Toyoki, and R. Nakatani, J. Phys.: Condens. Matter. **33**, 243001 (2021).
[17]E. J. Samuelson, M. T. Hutchings, and G. Shirane, Phys. Status Solidi B **48**, 13 (1970).
[18]X. Wang, K. Toyoki, R. Nakatani, and Y. Shiratsuchi, AIP Adv. **12**, 035216 (2022).
[19]T. Kosub, M. Kopte, F. Radu, O. G. Schmidt, and D. Makarov, Phys. Rev. Lett. **115**, 097201 (2015).
[20]Y. Ji, J. Miao, Z. Y. Ren, B. W. Dong, X. G. Xu, Y. Wu, and Y. Jiang, Appl. Phys. Lett. **110**, 262401 (2017).
[21]Y. Ji, J. Miao, Y. M. Zhu, K. K. Meng, X. G. Xu, J. K. Chen, and Y. Jiang, Appl. Phys. Lett. **112**, 232404 (2018).
[22]T. Moriyama, Y. Shiratsuchi, T. Iino, H. Aono, M. Suzuki, T. Nakamura, Y. Kotani, R. Nakatani, K. Nakamura, and T. Ono, Phys. Rev. Appl. **13**, 034052 (2020).
[23]S. Foner, Phys. Rev. **130**, 183 (1963).
[24]H. Hornreich and S. Shtrikman, Phys. Rev. **161**, 506 (1967).
[25]Z. Fang, N. Nagaosa, K. S. Takahashi, A. Asamitsu, R. Mathieu, T. Ogasawara, H. Yamada, M. Kawasaki, Y. Tokura, and K. Terakura, Science **302**, 92 (2003).
[26]R. Mathieu, A. Asamitsu, H. Yamada, K. S. Takahashi, M. Kawasaki, Z. Fang, N. Nagaosa, and Y. Tokura, Phys. Rev. Lett. **92**, 016602 (2004).
[27]Y. Onose and Y. Tokura, Phys. Rev. B **73**, 174421 (2006).
[28]D. Boldrin, I. Samathrakis, J. Zemen, A. Mihai, B. Zou, F. Johnson, B. D. Esser, D. W. McComb, P. K. Petrov, H. Zhang, and K. F. Cohen, Phys. Rev. Mater. **3**, 094409 (2019).
[29]J. Wang and C. Binek, Phys. Rev. Appl. **5**, 031001 (2016).
[30]C. N. Yang, Phys. Rev. **85**, 808 (1952).
[31]A. F. Andreev, Jetp. Lett. **63**, 758 (1996).
[32]K. D. Belashchenko, Phys. Rev. Lett. **105**, 147204 (2010).
[33]Y. Shiratsuchi, M. Suzuki, K. Toyoki, K. Wakatsu, T. Nishimura, T. Nakamura, and R. Nakatani, Physica B **583**, 412053 (2020).
[34]T. Iino, T. Moriyama, H. Iwaki, H. Aono, Y. Shiratsuchi, and T. Ono, Appl. Phys. Lett. **114**, 022402 (2019).
[35]Y. Shiratsuchi, Y. Tao, R. Tsutsumi, K. Toyoki, and R. Nakatani, J. Appl. Phys. **130**, 193902 (2021).
[36]P. Borisov, T. Ashida, T. Nozaki, M. Sahashi, and D. Lederman, Phys. Rev. B **93**, 174415 (2016).
[37]B. D. Cullity, *Elements of X-Ray Diffraction* (Addison-Wesley Publishing Company, 1967), pp.338–342.
[38]Y. Shiratsuchi, Y. Nakano, N. Inami, T. Ueno, K. Ono, R. Kumai, R. Sagayama, and R. Nakatani, J. Appl. Phys. **123**, 103903 (2018).
[39]W. Pies and A. Weiss, *Landolt-Börnsterin, New Series, Group III* (Springer-Verlag, Berlin, 1975), Vol. 7, p. 242.